

Spin Hall effect in iron-based superconducting materials: An effect of Dirac point

Sudhakar Pandey¹, Hiroshi Kontani¹, Dai S. Hirashima¹, Ryotaro Arita^{2,3}, and Hideo Aoki^{4,5}

¹*Department of Physics, Nagoya University, Furo-cho, Nagoya 464-8602, Japan*

²*Department of Applied Physics, University of Tokyo, Hongo, Tokyo 113-8656, Japan*

³*PRESTO, Japan Science and Technology Agency (JST), Kawaguchi, Saitama 332-0012, Japan*

⁴*Department of Physics, University of Tokyo, Hongo, Tokyo 113-0033, Japan*

⁵*TRIP(JST), 5 Sanbancho Chiyoda-ku, Tokyo 102-0075, Japan*

We have theoretically explored the intrinsic spin Hall effect (SHE) in the iron-based superconductor family with a variety of materials. The study is motivated by an observation that, in addition to an appreciable spin-orbit coupling in the Fe $3d$ states, a character of the band structure in which Dirac cones appear below the Fermi energy may play a crucial role in producing a large SHE. Our investigation does indeed predict a substantially large spin Hall conductivity in the heavily hole-doped regime such as KFe_2As_2 . The magnitude of the SHE has turned out to be comparable with that for Pt despite a relatively small spin-orbit coupling, which we identify to come from a huge contribution from the gap opening induced by the spin-orbit coupling at the Dirac point, which can become close to the Fermi energy for the heavy hole doping.

PACS numbers: 72.25.Ba, 74.25.Jb, 74.70.Xa, 75.47.-m

There is a mounting interest in the spin Hall effect, where a transverse spin current (as opposed to charge current) is induced in an electric field[1], which provides a most promising way for manipulating spin degrees of freedom for spintronic devices based on nonmagnetic materials. After its theoretical prediction in 1999 [2], which was originally proposed in 1971 [3], investigations were initially focused mostly in semiconductors[4]. More recently, attention has been extended toward metallic systems [5–15], following experimental reports of a huge spin Hall conductivity (SHC) $\sim 240\hbar e^{-1}\Omega^{-1}\text{cm}^{-1}$ in Pt [5] that is about 10^4 times larger than the reported values in semiconductors [4]. A key question then is how we can identify the materials that can exhibit large SHE.

Although SHE is driven by the spin-orbit interaction (SOI), understanding its mechanism in *metallic* systems, especially intrinsic vs extrinsic mechanisms, remains an open issue [1]. The intrinsic mechanism depends on the details of electronic structure and predicted to be realized when the residual resistivity is mainly contributed by the randomness of the crystal [6–12]. The extrinsic mechanism, on the other hand, is governed by external impurities in the host metallic system and becomes important when the impurity atoms with d - or f - orbital degree of freedom give the dominant scattering[14, 15]. Here we find that the intrinsic mechanism is dominant for the systems of our interest. This mechanism, apart from accounting for the observed huge SHC in Pt [6, 7, 9, 10], also predicts a variety of materials, such as several $4d$ and $5d$ transition metals [9, 10], as good candidates for SHE. Interestingly, many of these predictions have been realized recently in experiments [13].

In this Rapid Communication we explore the possibility of SHE in the recently discovered iron-based superconducting materials, such as iron pnictides and chalcogenides.

While the materials are now believed to be another class of high- T_c superconductors after cuprates [16], the reason why we look from the viewpoint of SHE is the following. These materials are typically *multiband* systems, where various d orbitals are involved in the conduction bands [17]. The bands are entangled, namely, cross with each other with different orbital characters as a consequence of crystal symmetries in the iron-based materials, a situation that leads to the occurrence of “Dirac cones” [18]. We have also an appreciable spin-orbit coupling (SOC) for the Fe $3d$ states and a quasi-two-dimensional nature of dispersion. Such features are expected to produce large SHE. For example, a large and quantized SHC is predicted in graphene when the Dirac cone becomes massive in presence of SOI[19]. Interestingly, the relatively strong strength of the SOC for the Fe $3d$ states (72meV) [20] in comparison to the case of graphene($\simeq 4\text{meV}$)[21] is also favorable for experimental realization of SHE in these materials.

This is our reasoning, and, if the Dirac points in these materials lead to a large SHE, then, apart from being a good candidate for spintronics, the materials may also provide an avenue for exploring the Dirac physics in the context of SHE in metallic systems that has recently drawn a surge of interests in case of topological insulators [22]. The present study does indeed predict a substantially large SHC for heavily hole-doped system such as KFe_2As_2 , whose origin, as expected, lies in the SOC-induced gap at Dirac points that lie almost at the Fermi level. We stress the Dirac-point-originated large SHE in the iron-based materials is distinct from other systems such as Pt and $4d$ and $5d$ transition metals, where substantially stronger SOC’s govern the behavior of SHE.

We consider the realistic band structure of various types of the iron compounds with two Fe atoms per unit

cell by incorporating the SOC within an effective tight-binding (TB) Hamiltonian. The Wannier basis of the TB model has been constructed as follows. We first performed a density-functional calculation, where we used the exchange correlation functional proposed by Perdew *et al.* [23], and the augmented plane wave and local orbital (APW+lo) method including the SOC as implemented in the WIEN2k code[24, 25]. We then constructed the TB model using the WIEN2Wannier[26] and the wannier90 [27]. In order to preserve the local symmetry of the Wannier functions, we perform the so-called one-shot Wannierization [28]. Our approach provides a good description of several common electronic features in these materials [29] such as an effective d -electron bandwidth of 4.5–5.0 eV, and the dominant orbital character of electronic states etc., which are almost independent of the SOC, as can be seen in Fig. 1, and expected from the weak SOC for the Fe $3d$ electrons. However, we shall discuss later that some SOC-induced band features in fact play a crucial role in the SHE.

Intrinsic mechanism based SHE is investigated with the linear-response theory[30] in the presence of local impurities that give rise to a finite residual resistivity. At $T = 0$, SHC consists of two parts, $\sigma_{xy}^z = \sigma_{xy}^{zI} + \sigma_{xy}^{zII}$, where

$$\sigma_{xy}^{zI} = \frac{1}{2\pi N} \sum_{\mathbf{k}} \text{Tr} \left[\hat{j}_x^S \hat{G}^R \hat{j}_y^C \hat{G}^A \right]_{\omega=0} \quad (1)$$

represents the ‘‘Fermi-surface term’’, while

$$\begin{aligned} \sigma_{xy}^{zII} = & -\frac{1}{4\pi N} \sum_{\mathbf{k}} \int_{-\infty}^0 d\omega \text{Tr} \left[\hat{j}_x^S \frac{\partial \hat{G}^R}{\partial \omega} \hat{j}_y^C \hat{G}^R \right. \\ & \left. - \hat{j}_x^S \hat{G}^R \hat{j}_y^C \frac{\partial \hat{G}^R}{\partial \omega} - \langle R \leftrightarrow A \rangle \right] \quad (2) \end{aligned}$$

represents the ‘‘Fermi-sea term’’. Here the charge-current operator is given by $\hat{j}_\zeta^C = -e\partial\hat{H}/\partial\mathbf{k}_\zeta$ with $-e (< 0)$ being the electronic charge, and $\zeta = x, y$, while the σ_z -spin current operator is given by $\hat{j}_\zeta^S = (-1/e)\{\hat{j}_\zeta^C, \hat{\sigma}_z\}/2$. The retarded (advanced) Green’s function $\hat{G}^R(\hat{G}^A)$ are given by $\hat{G}^{R/A}(\mathbf{k}, \omega) = 1/(\omega + \mu - \hat{H} \pm i\hat{\Gamma})$. Here \hat{H} is the effective TB Hamiltonian, a 20×20 matrix spanned by the two Fe atoms per unit cell in the presence of SOC, and μ the chemical potential. $\hat{\Gamma}$, the damping due to local impurities, is treated with the T-matrix approximation, $\hat{\Gamma} = (n_{\text{imp}}/2i)[\hat{T}(-i0) - \hat{T}(+i0)]$, where n_{imp} is the impurity concentration, and $\hat{T}(\pm i0) = \hat{I}/[1 - \hat{I}\hat{g}(\pm i0)]$, with $\hat{g}(\omega) = \sum_{\mathbf{k}} G(\mathbf{k}, \omega)$ representing the T-matrix for a single impurity with an impurity potential \hat{I} . For simplicity we consider a constant and orbital-diagonal impurity potential of strength I , i.e., $\hat{I}_{\alpha,\beta} = I\delta_{\alpha,\beta}$.

In the quantitative investigations that follow, our results for SHC are expressed in unit of $|e|/2\pi a$, where a is the interlayer spacing. For $a = 6\text{\AA}$, $|e|/2\pi a \sim$

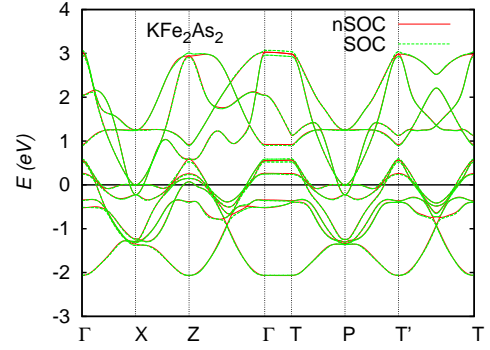


FIG. 1: Band structures with (SOC) and without (nSOC) spin-orbit coupling are shown for KFe_2As_2 . The symmetry points are: $\Gamma = (0, 0, 0)$, $X = (\pi, 0, 0)$, $Z = (\pi, \pi, 0)$, $T = (0, 0, \pi)$, $P = (\pi, 0, \pi)$, and $T' = (\pi, \pi, \pi)$. In our convention, $E = 0$ represents the chemical potential μ , and x – and y – are directed along the nearest neighbor Fe atoms.

$645\hbar e^{-1}\Omega^{-1}\text{cm}^{-1}$. Unless otherwise mentioned, we consider $I = 6$ eV, and $n_{\text{imp}} = 0.01$.

Figure 2 (a) shows the results for SHC for various materials, KFe_2As_2 , FeSe , and $\text{LaFeAsO}_{0.9}\text{F}_{0.1}$, obtained with the *ab initio* band structures. The dominant contribution is found to arise from the Fermi-surface part, i.e., $\sigma_{xy}^z \simeq \sigma_{xy}^{zI}$, for all the materials considered. While a large SHC arises in KFe_2As_2 , a heavily hole-doped system, it becomes vanishingly small in undoped FeSe and weakly electron-doped $\text{LaFeAsO}_{0.9}\text{F}_{0.1}$. Interestingly, the large magnitudes of $\text{SHC} \sim 1300\hbar e^{-1}\Omega^{-1}\text{cm}^{-1}$ in KFe_2As_2 with a residual resistivity $\rho \sim 10\mu\Omega\text{cm}$ is comparable to that ($\sim 1000\hbar e^{-1}\Omega^{-1}\text{cm}^{-1}$) predicted for Pt with a substantially larger SOC in the same metallic regime, where the observed $\text{SHC} \sim 240\hbar e^{-1}\Omega^{-1}\text{cm}^{-1}$ is reproduced at higher $\rho \sim 100\mu\Omega\text{cm}$ [6, 9, 10]. We trace the origin of the large SHC in KFe_2As_2 in a special band feature later.

Since the SHE is found to be significantly affected by the doping level, we next investigate the effect of carrier doping by varying the band filling over a range ($n = 5.5 - 6.5$) that goes from electron doped ($n > 6$) to hole doped ($n < 6$) sides as relevant to the family of these materials. We follow a rigid-band approach using the band structure of BaFe_2As_2 that is known to cover both electron doping as in $\text{Ba}(\text{Fe}_{1-x}\text{Co}_x)_2\text{As}_2$ and hole doping as in $\text{Ba}_{1-x}\text{K}_x\text{Fe}_2\text{As}_2$. Here we only consider the Fermi-surface part, which is found to be dominant as discussed above. The result, a curve in Fig. 2 (a), exhibits a large SHC in the heavily hole-doped regime ($n \simeq 5.5$), while the magnitude is small in the weakly hole-doped and electron-doped regimes. The overall filling dependence agrees with the results for KFe_2As_2 ($n = 5.5$), FeSe ($n = 6.0$), and $\text{LaFeO}_{0.9}\text{F}_{0.1}$ ($n = 6.1$), and highlights the presence of a common feature. Small deviations from the rigid-band result should be due to deformations in the electronic structures, such as the stronger three dimensionality in BaFe_2As_2 .

As for the dependence on the impurity potential

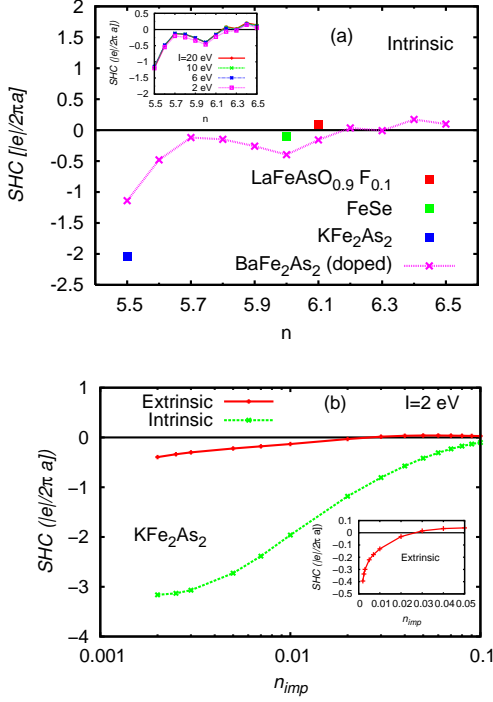


FIG. 2: (a) Intrinsic mechanism based results for SHC for various systems (symbols). The curve is the doping dependence in the rigid-band approximation for the band structure of BaFe_2As_2 . Inset shows the dependence of the result on the strength of impurity potential. (b) Relative contributions of the intrinsic (σ_{xy}^I) and extrinsic (σ_{xy}^{ss}) mechanism to SHC as a function of impurity concentration (n_{imp}), as shown for KFe_2As_2 . Here inset demonstrates the rapid increase of the extrinsic mechanism in the limiting case $n_{imp} \rightarrow 0$

strength, we have checked, as shown in the inset of Fig. 2 (a), that, when we vary the strength over ($I \sim 2 - 20$) eV, the SHC, including its filling dependence, is rather insensitive to the strength of impurity potential[31]. This hallmarks an intrinsic nature of SHE in these materials.

In order to further support our prediction for the intrinsic origin of SHE, we now estimate the contribution of extrinsic mechanism by focusing on the skew scattering term[14], $\sigma_{xy}^{ss} = \frac{n_{imp}}{2} \frac{1}{2\pi} \sum_{l,m,n,o} [B_{m,n} T_{n,l}^R A_{l,o} T_{o,m}^A + c.c.]$ with $A_{l,m} = \sum_k [G^R J_y^C G^A]_{l,m}$ and $B_{l,m} = \sum_k [G^A J_x^S G^R]_{l,m}$, which is predicted to be dominant in the limit of dilute impurities[14]. As shown in Fig. 2 (b), the contribution of skew scattering is nearly smaller by an order of magnitude in comparison to that of the intrinsic part for $n_{imp} \sim 0.01$. For $n_{imp} < 0.01$, while intrinsic contribution tends to saturate, the skew scattering contribution increases rapidly in proportion to $1/n_{imp}$. The two contributions become comparable in the regime $n_{imp} < 0.001$, where $\rho \leq 1\mu\Omega\text{cm}$. Since such a high quality sample is very difficult to prepare experimentally, we believe that the intrinsic contribution is dominant in "realistic" clean samples with $\rho \geq 10\mu\Omega\text{cm}$.

In the following our discussion will be based on the intrinsic mechanism with a focus on the heavily hole-doped system KFe_2As_2 that exhibits the large SHC. In view of the dominant contribution from the

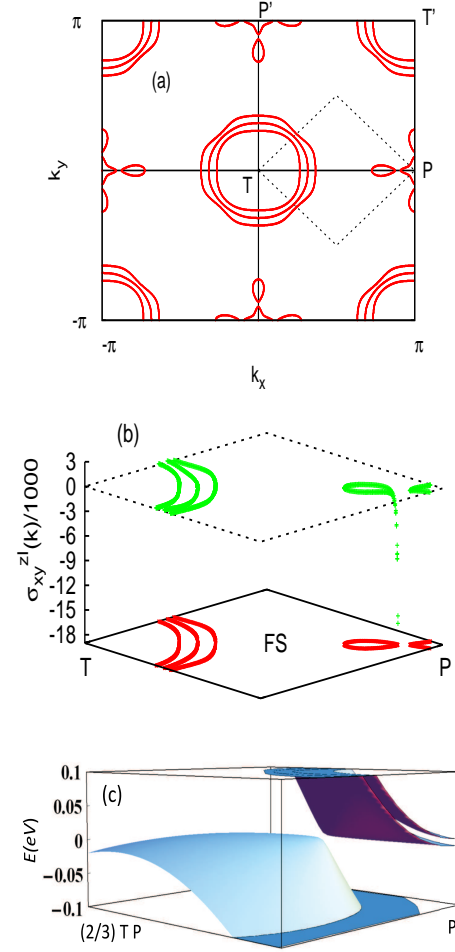


FIG. 3: (a) Fermi surface for KFe_2As_2 shown on the $k_z = \pi$ plane. (b) \mathbf{k} -dependent contribution from the states on the Fermi surface (red lines) to SHC (green), displayed for a part of Fermi surface (dotted region in (a)). Here dotted region represents the $\sigma_{xy}^{zI}(\mathbf{k}) = 0$ plane. (c) Gapped Dirac cone dispersion near P. Electronic states make the huge contribution to SHC (b) in the close vicinity of the gap.

Fermi surface part (σ_{xy}^{zI}) we explore if certain special band features around the Fermi energy are responsible. We consider the \mathbf{k} -dependent contribution of electronic states on the Fermi surface to SHC, $\sigma_{xy}^{zI}(\mathbf{k}) = \frac{1}{8} \sum_{k'=\pm k_x, \pm k_y, \pm k_z} \text{Tr}[(\hat{J}_x^S \hat{G}^R \hat{J}_y^C \hat{G}^A - \hat{J}_y^S \hat{G}^R \hat{J}_x^C \hat{G}^A)/2]_{k',\omega=0}$ where we are averaging over xy and yx components etc., with $\frac{1}{2\pi N} \sum_{\mathbf{k}} \sigma_{xy}^{zI}(\mathbf{k})$ providing the net contribution of σ_{xy}^{zI} [6].

We consider only a part of the Brillouin zone, as shown by the dotted area in Fig. 3 (a), as the other parts can be deduced from the symmetry. For clarity we consider the $k_z = \pi$ plane, as other planes give qualitatively similar contributions due to quasi-2D nature of the Fermi surface that is also apparent from the almost flat dispersion near the Fermi level along $\Gamma - T$ direction (Fig. 1). Figure 3 (b) shows that a huge contribution to SHC comes from a small region on the hole pocket near P, while the contributions from the rest part are not only

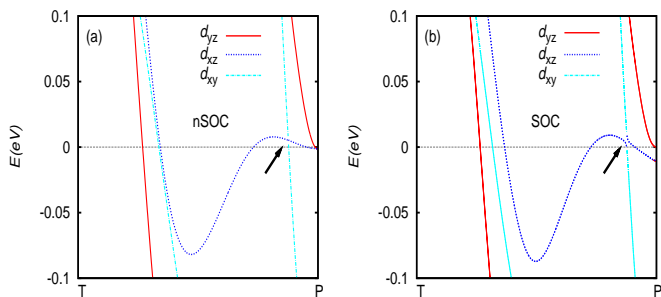


FIG. 4: Band dispersions for KFe_2As_2 around the Fermi level ($E = 0$) without SOC (a) and with SOC (b). The Dirac point, around which dominant contributions to SHC arise as shown in Fig. 3, is indicated with arrows. The small gap ($\ll \text{SOC}$) is reflected more clearly in Fig 3(c) due to tilted nature of the Dirac cone.

relatively much smaller but also tend to cancel with each other. Therefore, origin of the large SHC is governed by the states on the hole pocket near P.

We can actually identify, in Figures 3 (c) and 4, that these electronic states lie in the close vicinity of a small SOC-induced gap in the Dirac cone. This is also the case with our analysis for the filling dependence in BaFe_2As_2 with a rigid band, where we find a similar origin behind the large SHC in the heavily hole-doped regime ($n \simeq 5.5$), in which the Fermi level approaches the Dirac point. Concomitantly, such Dirac-like points near the Fermi level are absent in FeSe and $\text{LaFeAsO}_{0.9}\text{F}_{0.1}$. Thus the large SHC when the Fermi level lies close to the SOC-induced gap at the Dirac point renders the iron-based systems a Dirac electron system such as graphene[19].

Such Dirac-like points arise due to crossing of two bands with almost linear dispersions and different orbital characters as a consequence of crystal symmetries in the iron-based materials. In the present case, while one of the crossing bands has dominantly xz orbital character, the other band has xy character (Fig. 4). The band crossing is a consequence of the opposite parities of the two orbitals with respect to reflection $y \rightarrow -y$. In the presence of an SOI, the gap opens because the two orbitals are then coupled by the x -component of the orbital angular momentum \hat{l}_x ; $\langle xz | \hat{l}_x | xy \rangle = i$ [9].

We also study the temperature dependence of SHC in KFe_2As_2 . As expected from the small SOC-induced gap at the Dirac point, the SHC decreases monotonically, and at room temperature (300K), it reduces to about 60% of its $T = 0$ value that is still significantly large and favorable for device application.

Although it is an important future problem to study the role of correlation effects on the SHC, we expect that it is less important in Fe-based superconductors as follows: The Coulomb interaction is much smaller than the bandwidth according to the first principle study by Miyake *et al.* [29], consistently with the small mass-enhancement factor $m^*/m = 2 \sim 3$. Note that the

SHC is independent of the mass-enhancement [11]. Although spin fluctuations can sensitively influence transport phenomena[32], spin fluctuations in KFe_2As_2 are small according to $1/T1$ measurements, due to the bad nesting of the Fermi surface. Thus we expect that the giant SHC in KFe_2As_2 , which is the most important result of our study, will be reliable.

In summary, we have theoretically explored the possibility of SHE in a variety of the iron-based superconducting materials. We reveal that a substantially large SHE arises in heavily hole-doped materials of 122 family such as KFe_2As_2 , whose magnitude is even comparable with that in Pt. The large SHE is found to originate from a huge contribution from the electronic states in the vicinity of the SOC-induced gap at the Dirac points that lie close to the Fermi level in the heavily hole doped case. We hope that our study will stimulate an experimental investigation due to relative easiness in synthesis and higher sample quality of the 122 family of materials.

S. P. and R. A. are supported by the JSPS Postdoctoral Fellowship for Foreign Researchers, and the JST PRESTO program, respectively.

-
- [1] For a recent review, see, e.g., G. Vignale, *J. Supercond. Nov. Magn.*, **23**, 3 (2010).
 - [2] J. E. Hirsch, *Phys. Rev. Lett.* **83**, 1834 (1999).
 - [3] M. I. D'yakonov, and V. I. Perel', *JETP Lett.* **13**, 467 (1971); *ibid.* *Phys. Lett. A* **35**, 459 (1971).
 - [4] Y. Kato *et al.*, *Science* **306**, 1910 (2004).
 - [5] T. Kimura *et al.*, *Phys. Rev. Lett.* **98**, 156601 (2007).
 - [6] H. Kontani *et al.*, *J. Phys. Soc. Jpn.* **76**, 103702 (2007).
 - [7] G. Y. Guo *et al.*, *Phys. Rev. Lett.* **100**, 096401 (2008).
 - [8] H. Kontani *et al.*, *Phys. Rev. Lett.* **100**, 096601 (2008).
 - [9] T. Tanaka *et al.*, *Phys. Rev. B* **77**, 165117 (2008).
 - [10] H. Kontani *et al.*, *Phys. Rev. Lett.* **102**, 016601 (2009).
 - [11] T. Tanaka *et al.*, *Phys. Rev. B* **81**, 224401 (2010).
 - [12] A. Fert *et al.*, *Phys. Rev. Lett.* **106**, 157208 (2011).
 - [13] M. Morota *et al.*, *Phys. Rev. B* **83**, 174405 (2011).
 - [14] T. Tanaka *et al.*, *New J. Phys.* **11**, 013023 (2009).
 - [15] G. Y. Guo *et al.*, *Phys. Rev. Lett.* **102**, 036401 (2009).
 - [16] See, e.g., F. Wang *et al.*, *Science* **332**, 200 (2011).
 - [17] K. Kuroki *et al.*, *Phys. Rev. Lett.* **101**, 087004 (2008); *ibid.* **102**, 109902(E) (2009); *Phys. Rev. B* **79**, 224511 (2009).
 - [18] O. K. Andersen *et al.*, *Annalen der Physik*, **523**, 8 (2011).
 - [19] C. L. Kane *et al.*, *Phys. Rev. Lett.* **95**, 146802 (2005).
 - [20] T. Naito *et al.*, *Phys. Rev. B* **81**, 195111 (2010).
 - [21] Y. Yao *et al.*, *Phys. Rev. B* **75**, 041401 (2007).
 - [22] M. Z. Hasan *et al.*, *Rev. Mod. Phys.* **82**, 3045 (2010).
 - [23] J. P. Perdew *et al.*, *Phys. Rev. Lett.* **77**, 3865 (1996).
 - [24] P. Blaha *et al.*, <http://www.wien2k.at/>
 - [25] J. Kunes *et al.*, *Phys. Rev. B* **64**, 153102 (2001).
 - [26] J. Kunes *et al.*, *Comput. Phys. Commun.* **181**, 1888 (2010).
 - [27] A. A. Mostofi *et al.*, *Comput. Phys. Commun.* **178**, 685 (2008).
 - [28] As for the full minimization of the size of the Wannier

- functions, see N. Marzari *et al.*, Phys. Rev. B **56**, 12847 (1997); I. Souza *et al.*, *ibid.* **65**, 035109 (2001).
- [29] See, e.g., T. Miyake *et al.*, J. Phys. Soc. Jpn, **79**, 044705 (2010).
- [30] P. Streda, J. Phys. C **15** L717 (1982).
- [31] K. Nakamura *et al.*, Phys. Rev. B **83**, 144512 (2011), have estimated the impurity potential strengths for various elements, which lie around $|I| \sim 8$ eV.
- [32] H. Kontani, Rep. Prog. Phys. **71**, 026501 (2008).